Nano Res. 2011, 4(9): 891–900
DOI 10.1007/s12274-011-0145-6
Research Article

ISSN 1998-0124
CN 11-5974/O4

Graphene–CdSe Nanobelt Solar Cells with Tunable Configurations

Luhui Zhang[1], Lili Fan[2], Zhen Li[2], Enzheng Shi[1], Xinming Li[2], Hongbian Li[1], Chunyan Ji[1], Yi Jia[2], Jinquan Wei[2], Kunlin Wang[2], Hongwei Zhu[2,3] (✉), Dehai Wu[2], and Anyuan Cao[1] (✉)

[1] Department of Advanced Materials and Nanotechnology, College of Engineering, Peking University, Beijing 100871, China
[2] Key Laboratory for Advanced Materials Processing Technology and Department of Mechanical Engineering, Tsinghua University, Beijing 100084, China
[3] Center for Nano and Micro Mechanics, Tsinghua University, Beijing 100084, China

Received: 15 February 2011 / Revised: 10 March 2011 / Accepted: 27 April 2011

ABSTRACT

We have combined two planar nanostructures, graphene and CdSe nanobelts, to construct Schottky junction solar cells with open-circuit voltages of about 0.5 V and cell efficiencies on the order of 0.1%. By covering transparent graphene or carbon nanotube (CNT) films on selected positions along macroscopically long CdSe nanobelts, we have demonstrated the fabrication of active solar cells with many different configurations and parallel connections from individual or multiple assembled nanobelts. The graphene–CdSe nanobelt solar cells reported here show a great flexibility in creating diverse device architectures, and might be scaled up for cell integration based on assembled nanobelt arrays and patterned graphene (or CNT) films.

KEYWORDS

Graphene, CdSe nanobelts, solar cells, Schottky junction

1. Introduction

Semiconducting nanowires, graphene and carbon nanotubes (CNTs) are basic platforms to build nanoelectronic and optoelectronic devices [1–4]. Owing to their one- or two-dimensional shapes, long-range uniformity and controlled modulation of electronic properties, small-scale device coupling such as tandem solar cells and logic circuits along individual nanostructures has been demonstrated [5, 6]. Graphene films can be patterned as nanomeshes or tailored into nanoribbons to form semiconducting films and high performance transistors [7, 8]. Furthermore, synthesis and self-assembly techniques developed in recent times can produce continuous centimeter-long nanowires/nanotubes and transparent graphene films with large areas, as well as make ordered vertical or horizontal arrays [9–14]. This progress is very promising for the development of large-scale integrated nanodevices, which represents an important step towards practical applications.

Involving nanostructures in photovoltaic devices not only provides a rich selection of high quality materials for investigating optical and electrical properties, but also leads to a variety of tailored structures that could potentially reach high energy conversion efficiency, including depleted quantum dot heterojunctions, graphene and nanoparticle hybrid layers, core–shell nanocables, and three-dimensional nanowire arrays [15–20]. It was found that covering a CdS

Address correspondence to Anyuan Cao, anyuan@pku.edu.cn; Hongwei Zhu, hongweizhu@tsinghua.edu.cn

nanowire with a graphene film results in a device with evident photocurrent under illumination [21]. However, this improved solar cell was based on junctions between the CdS nanowire and a metal film (Au) rather than graphene [22]. In addition to nanowires, nanobelts have a comparable aspect ratio but much larger widths up to tens of micrometers [23], resulting in an unique flat surface on which smooth layers can be deposited to form heterojunctions. Building junctions from a wide nanobelt surface could potentially lead to flexible thin film devices, which has been rarely reported, whereas nanowire-based junctions have been more intensively studied. Recently, we reported CNT–CdSe nanobelt Schottky junction solar cells [24]. Compared with CNT films which have a porous network, graphene has the advantage of being able to give 100% coverage and contact to nanobelts.

2. Experimental

CdSe nanobelts were synthesized by a chemical vapor deposition (CVD) process [24]. Few-layer graphene films were grown on copper foils by a self-catalytic CVD method. The device fabrication process involves three main steps: nanobelt deposition, graphene transfer and Ag paste contacting. First, a single CdSe nanobelt was picked from the growth substrate and deposited onto a glass slide. Second, a piece of graphene film floating on a water surface was laid down on one end of the nanobelt, covering about one third to two thirds of the nanobelt length. Finally, Ag paste was applied to the other end of the nanobelt as the negative electrode, with a controlled distance to the graphene film edge. Devices with various configurations were fabricated by combining graphene films with one or two CdSe nanobelts at selected positions. Details of the synthesis parameters and fabrication methods are included in the Electronic Supplementary Material (ESM).

The morphology and structure of the CdSe nanobelts and solar cells were characterized by optical microscope (Olympus BX51M), scanning electron microscope (SEM) (Hitachi S4800) and transmission electron microscope (TEM) (JEOL JEM-2010). Raman spectroscopy was performed with a LabRam ARAMIS confocal micro Raman spectrometer with an excitation laser wavelength of 532 nm. Solar cell tests were carried out with a solar simulator (Newport Thermo Oriel 91195A-1000) under AM 1.5G condition at an illumination intensity of 100 mW/cm^2, calibrated by a standard Si solar cell (91150V). In all the cells, the graphene or CNT film was wired as the positive electrode and the Ag paste connecting the nanobelt as the negative electrode. All current–voltage (I–V) data were recorded using a Keithley 2635A SourceMeter.

3. Results and discussion

Here, we combine graphene films with semiconducting CdSe nanobelts to fabricate Schottky junction solar cells, in which the nanobelt surface is coated by a graphene sheet as the transparent electrode (Fig. 1(a)). Because both materials can be considered as a two-dimensional flat structure, their contact actually results in a planar device which can be further modified into various configurations and connected in parallel. As illustrated in Fig. 1(b), the working principle of this cell can be described in the following steps. First, under light illumination, the CdSe nanobelt with a bandgap of ~1.74 eV is excited and free electrons/holes are produced. Then, the charge carriers diffuse to the region of built-in electric field at the CdSe–graphene interface where they are separately accelerated along different directions. The energy band diagram across the interface shows a Schottky junction and the presence of an electric field (qV_D ~0.5 eV) which directs electrons to the CdSe and holes to the graphene side (Fig. 1(c)). In the final step, electrons are transported through the nanobelt to the negative electrode, and holes flow through the graphene film to the positive electrode, respectively. Because of the absence of opaque metal electrodes through the cross-section of the cell, the device can work under illumination from either the graphene or nanobelt side.

Figure 1(d) shows the optical picture of a graphene–CdSe solar cell in which the right portion (~2.2 mm long) of the nanobelt is covered by a large-area graphene film and the left end is contacted by silver (Ag) paste for electrical wiring. The few-layer graphene film (Fig. S-1 in the ESM) has an optical transmittance of 90% at a wavelength of 550 nm and a sheet resistance of about 1500 Ω. The profile of the CdSe nanobelt underneath can be clearly seen from the graphene side.

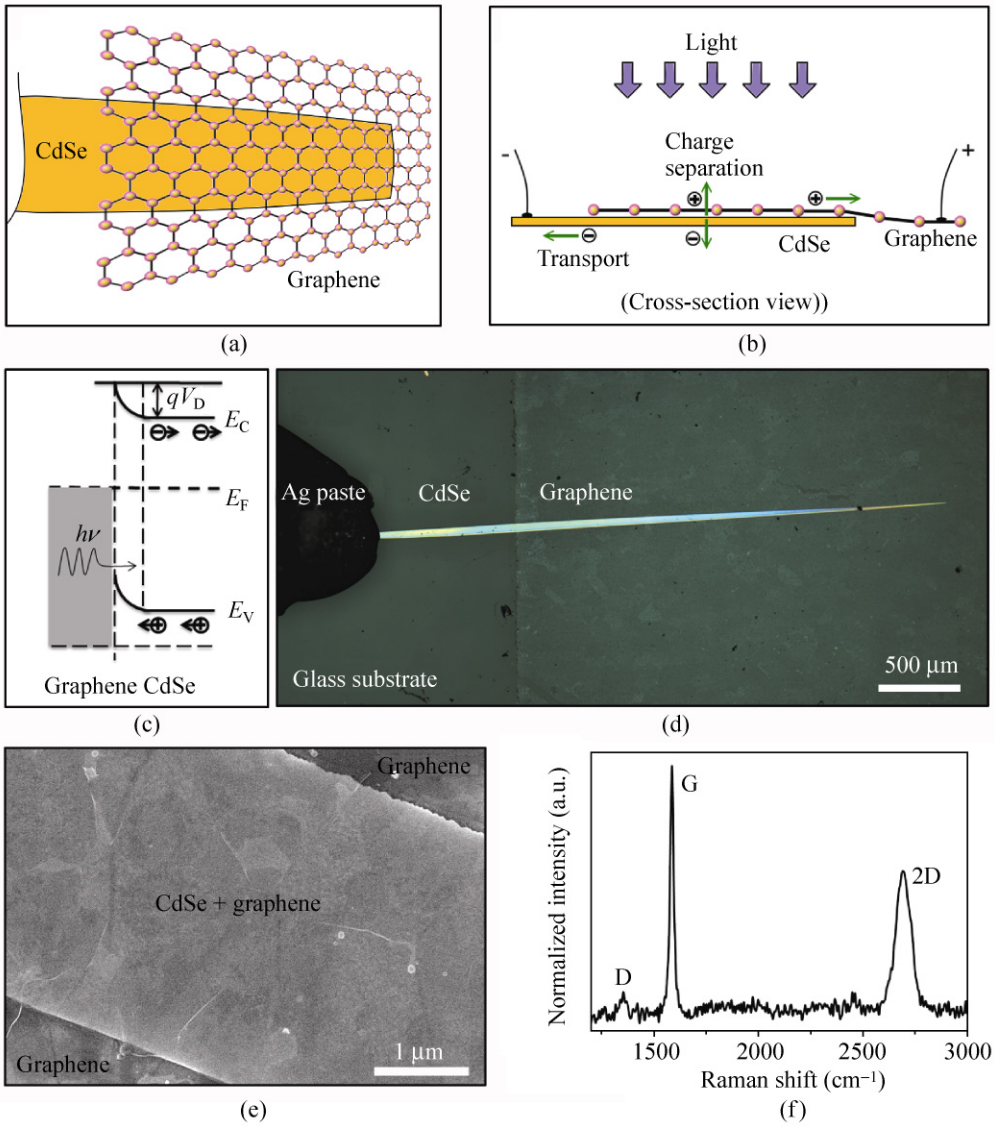

Figure 1 Structure of graphene–CdSe nanobelt Schottky junction solar cells. (a) Illustration of a single-layer graphene covered on the top surface of a CdSe nanobelt. The overlapped area forms the junction that is responsible for charge separation. (b) Cross-section view of the graphene–CdSe junction, showing the transport of electrons through the nanobelt, and holes through the graphene layer. (c) Energy band diagram across the graphene–CdSe interface. (d) Optical image of a solar cell consisting of a 3.5 mm-long nanobelt, a transparent graphene film covering about 2/3 of the nanobelt length, and Ag paste contact at the other end. (e) SEM image of the cell showing the graphene layer coated on the top surface of the nanobelt. (f) Raman spectrum of the graphene film with an excitation wavelength of 532 nm

SEM characterization shows that the graphene film has tightly wrapped around the nanobelt, forming a uniform and conformal coating on the nanobelt surface (Fig. 1(e)). The intimate contact between these two materials is very important for creating a sharp interface and junction. The Raman spectrum of the graphene film reveals its few-layer structure with a small percentage of defects (Fig. 1(f)).

The graphene–CdSe cell behaves as a diode when measured in the dark with an ideality factor (n) larger than three, and appreciable leakage current under reverse bias due to interfacial recombination (Fig. 2(a)). Under standard illumination conditions (AM 1.5G, 100 mW/cm^2) from the graphene side, this cell shows an open-circuit voltage (V_{oc}) of 0.49 V, a short-circuit current density (J_{sc}) of 0.94 mA/cm^2, and a power

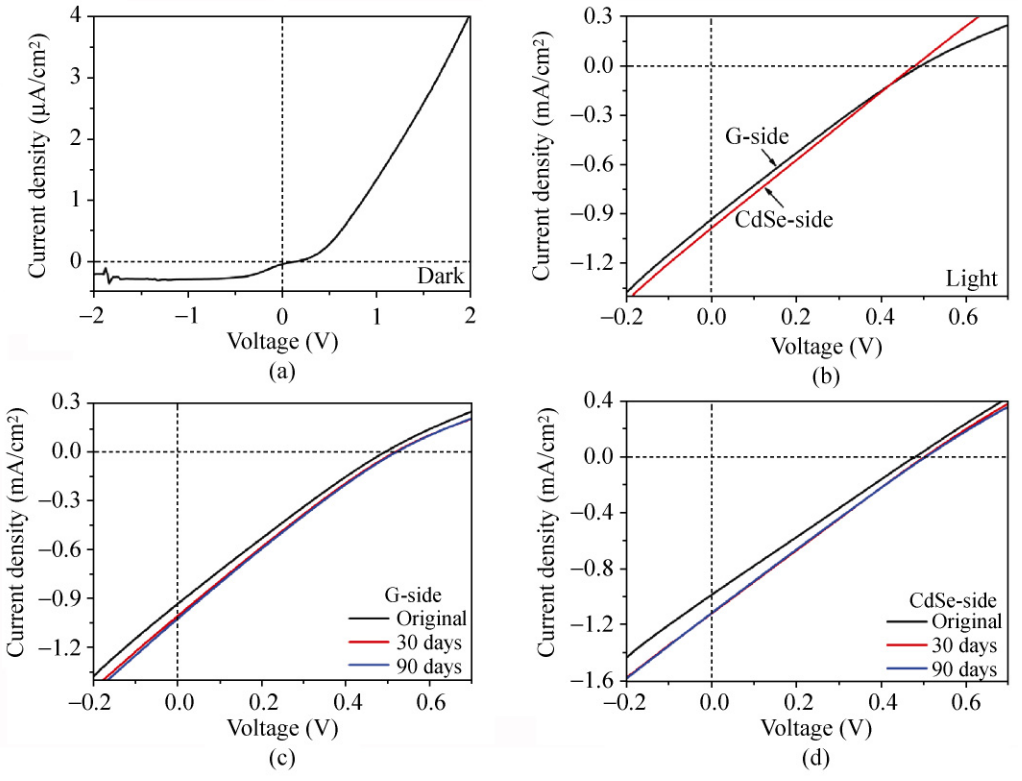

Figure 2 *J–V* characteristics of the graphene–CdSe solar cell: (a) dark *J–V* curve of a typical cell showing rectifying diode behavior; (b) *J–V* curves recorded when the cell was illuminated from the front (graphene film) side or from the back (nanobelt) side, with measured V_{oc} values of 0.49 and 0.48 V, J_{sc} of 0.94 and 1 mA/cm^2, and η of 0.11 % and 0.12 %, respectively; (c), (d) *J–V* curves of the same cell stored in air recorded during a period of three months under front or back side illumination

conversion efficiency (η) of 0.11% in which the graphene–CdSe overlapping region (junction) is considered as the active device area (where charge separation mainly occurs) (Fig. 2(b)). The relatively low fill factor (FF, < 23.7%) indicates there is considerable series resistance present in the current cell, which probably stems from the graphene film (sheet resistance), the CdSe nanobelt (path for electron transport), and the contact resistance between nanostructures and electrodes. When illuminated from the other (CdSe) side, the cell shows similar current density–voltage (*J–V*) characteristics with a V_{oc} of 0.48 V, J_{sc} of 1 mA/cm^2 and η of 0.12%, indicating that our cells can work under illumination from both sides without sacrificing device efficiency.

Because even a single-layer graphene is impermeable to atoms or gas molecules, the cell junction is well protected by the graphene film covered on the top. The graphene-covered cell shows excellent stability when placed in air for more than three months, without degradation of V_{oc}, J_{sc} or η (Figs. 2(c) and 2(d)). A slight increase in cell efficiency under illumination from both the graphene (from 0.11% to 0.12%) and CdSe (0.12% to 0.14%) sides was observed, due to the oxygen adsorption, and doping of the graphene layer and increase of hole carrier density. After a certain period and saturation of adsorption, the cell performance remained stable up to 90 days in air. In addition to rigid substrates (e.g., glass, wafer), CdSe nanobelts and graphene films can be deposited on flexible plastics such as polydimethylsiloxane (PDMS) to make solar cells (Fig. S-2 in the ESM).

Our device structure dictates that free electrons pass through the CdSe nanobelt to the negative electrode over a distance of δ, which can be predefined during the cell fabrication process (Fig. 3(a)). This portion of nanobelt is a source of series resistance, and also leads to more charge recombination. We have investigated the influence of this distance on the cell property, by varying the value of δ over a wide range in the same

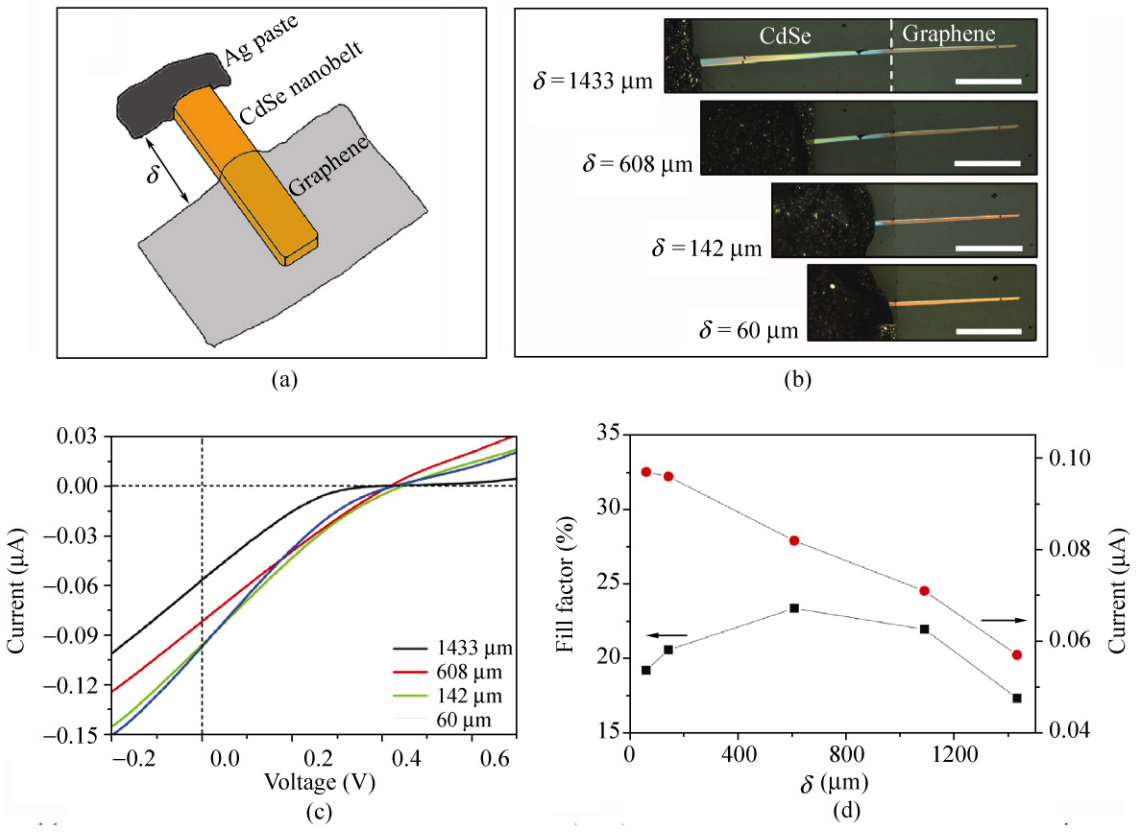

Figure 3 Solar cells with controlled nanobelt span (δ) between the Ag electrode and graphene film. (a) Illustration of the cell structure where δ is the distance between the Ag paste and the edge of the graphene film. (b) Optical images of four modified versions based on the same cell, in which Ag paste was applied progressively forwards and δ was reduced from about 1.5 mm down to 60 μm. The dashed line indicates the edge of the graphene film. (c) *I*–*V* curves of four solar cells with different δ values. (d) Calculated fill factors and short-circuit current values as a function of δ

graphene–CdSe junction cell. The Ag paste as electrode was applied to the left end of the nanobelt at an initial distance of 1433 μm from the edge of the graphene film, and progressively moved forward until δ = 60 μm (Fig. 3(b)). The *I*–*V* characteristics showed that the short-circuit current (I_{sc}) increased from 0.06 μA to 0.10 μA and then saturated when δ became smaller than 150 μm, indicating reduced charge recombination at shortened electron transport distances (Fig. 3(c)). The fill factors remained at a low level (15% to 25%) in most of the cells (Fig. 3(d)), mainly due to the relatively high resistance (on the order of MW) of the intrinsic CdSe nanobelts synthesized here. Because the junction area at the right part of the nanobelt was not affected, the V_{oc} value remained stable (0.42 V) in all tests. The values of I_{sc} and η might be further improved by reducing the electrode-to-junction distance down to several micrometers or less by photolithography. These results indicate that although its overall size is at millimeter scale, the solar cell has the potential to be miniaturized to a much smaller size (micro- or nanoscale) with improved performance.

The combination of graphene and long nanobelts results in the fabrication of different cell structures with great flexibility. For example, when a strip of graphene film was laid down on a nanobelt to form a cross junction, four active solar cells can be obtained simultaneously by defining the Ag paste contacts connected to the nanobelt ends as two negative electrodes (N1 and N2) and the two parts of graphene film (divided by the nanobelt) as positive electrodes (G1 and G2) (Fig. 4(a)). In this configuration, cells with different electrode pairs can be defined as G1–N1, G2–N1, G1–N2 and G2–N2, all of which share the same graphene–CdSe junction. Measured *I*–*V* curves show that two of the cells (G1–N1, G2–N1) have very similar

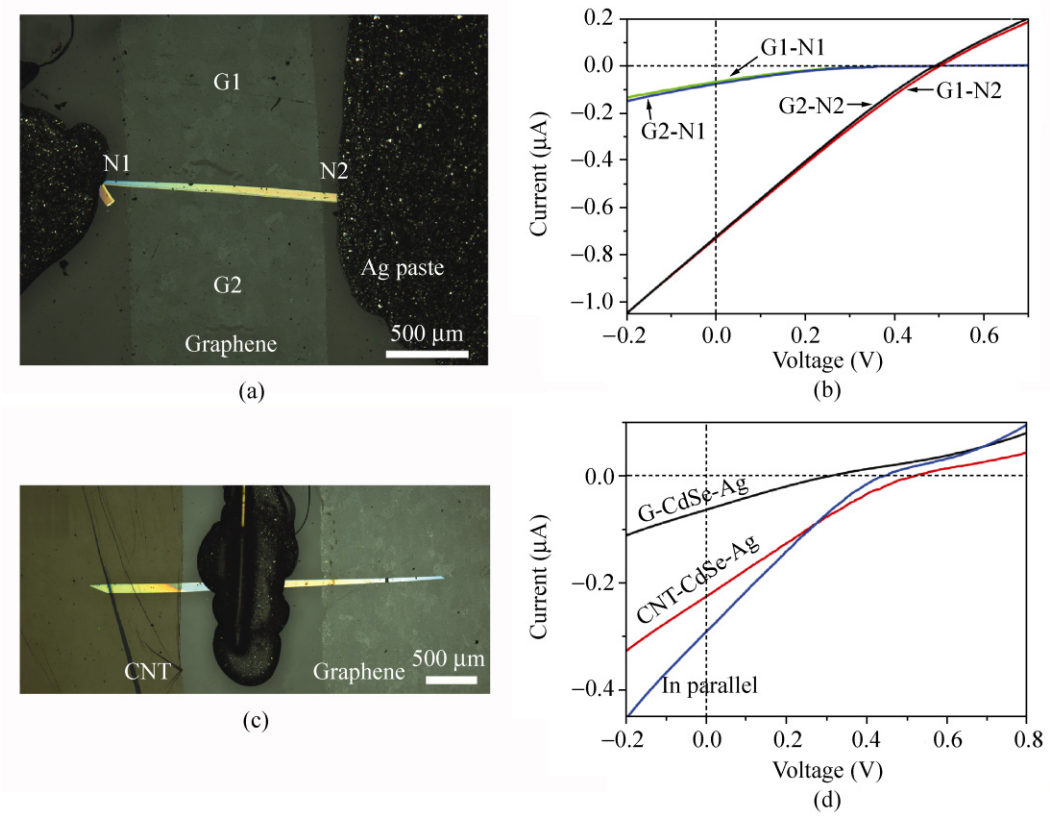

Figure 4 Two types of cell configurations based on a single nanobelt. (a) Optical image of a cross junction made by placing a strip of graphene film perpendicularly across a nanobelt. Different parts of the graphene film (G1, G2) and the nanobelt ends (N1, N2) can be paired selectively to form solar cells. (b) *I–V* curves of four cells with different electrode pairs. (c) Optical image of a nanobelt partially covered by a CNT and graphene film at its two ends, with Ag paste in the middle. (d) *I–V* curves of the CNT–CdSe–Ag cell, the graphene–CdSe–Ag cell, and two cells connected in parallel

characteristics, while the other two (G1–N2, G2–N2) have similar behavior (Fig. 4(b)). Cells G1–N1 and G2–N1 share the same nanobelt electrode (N1) but have different graphene parts (G1, G2). Their similar *I–V* curves indicate that the graphene film is uniform. If we compare cell G1–N1 with G1–N2, both have a V_{oc} of 0.45 V but there is a large difference between I_{sc}, which is 0.1 μA for G1–N1 and 0.5 μA for G1–N2. The difference in I_{sc} stems from the different widths of the nanobelt portions connecting to the Ag paste in each cell. The nanobelt portion between the Ag paste and the graphene film has an average width of 30 μm in cell G1–N1, and a width of 60 μm in cell G1–N2. With increasing uniformity of nanobelts through more controlled synthesis and better metal contacts (other than Ag paste), the reproducibility of our solar cells should be substantially improved.

We also can arrange different active junctions on a single nanobelt by covering a CNT and graphene film on its two ends, and using Ag paste in the middle as a common negative electrode (Fig. 4(c)). In this case, two solar cells are formed, and their structures can be defined as CNT–CdSe–Ag and G–CdSe–Ag. We noticed that the CNT–CdSe–Ag cell has a higher V_{oc} (0.52 V) than that of the G–CdSe–Ag cell (0.31 V), based on the same nanobelt (Fig. 4(d)). It indicates that the built-in electric fields at the CNT–CdSe and G–CdSe interfaces may be different, due to the work function difference between CNTs (~4.8 eV) and graphene (4.66 eV) [25]. The two cells also show different I_{sc} values. Parallel connection can be realized by joining the CNT and graphene film together as the positive electrode, which results in an intermediate value of V_{oc} (0.44 V) and a total I_{sc} which is the sum of those in each cell (Fig. 4(d)). In addition, we have used only graphene films to create two G–CdSe–Ag cells on a single nanobelt with a symmetric structure, as well as their parallel connection (Fig. S-3 in the ESM).

We have covered a graphene film on two separate CdSe nanobelts (N1 and N2) to make parallel solar cells, labeled as G–N1–Ag and G–N2–Ag, respectively (Fig. 5(a)). The graphene film acts as the common positive electrode for both cells. Although here the distance between the two nanobelts is more than 1 mm obtained by manual placement, higher density nanobelt arrays can be fabricated using self-assembly techniques for aligning nanowires [26–28]. Measurements on separate cells and their parallel connection reveal consistent behavior, with a constant V_{oc} and a total I_{sc} (0.18 μA) being the sum of the cell G–N1–Ag (0.13 μA) and G–N2–Ag (0.05 μA) (Fig. 5(b)). Since the cell G–N1–Ag has a much larger G–N1 junction area (~0.145 mm^2) compared with that of G–N2–Ag (0.046 mm^2), its output current is also higher. The current level is simply controlled by the width of the nanobelt and the resulting junction area. However, if we calculate the current density, then the two cells and their parallel connect have very similar J_{sc} values (Fig. 5(c)), indicating consistent behavior in the same batch of devices.

Finally, we have put the CdSe nanobelts in series connection and investigated the current degradation in solar cells with a larger number of nanobelts. Two individual nanobelts (N1 and N2) were placed on the substrate sequentially, and N1 went through N2 from its top surface forming a close contact in the middle of N2 (Figs. 6(a) and 6(b)). A graphene film was covered on the right end of N1, but without touching the other nanobelt (N2). Two electrodes were separately connected through Ag paste to the ends of nanobelt N1 and N2. In this configuration, measurement can be done either on the cell G–N1–Ag, or G–N1–N2–Ag, as illustrated in Fig. 6(c). For the latter cell, free electrons generated from the G–N1 junction have to flow through N1 and N2 to reach the Ag electrode, and

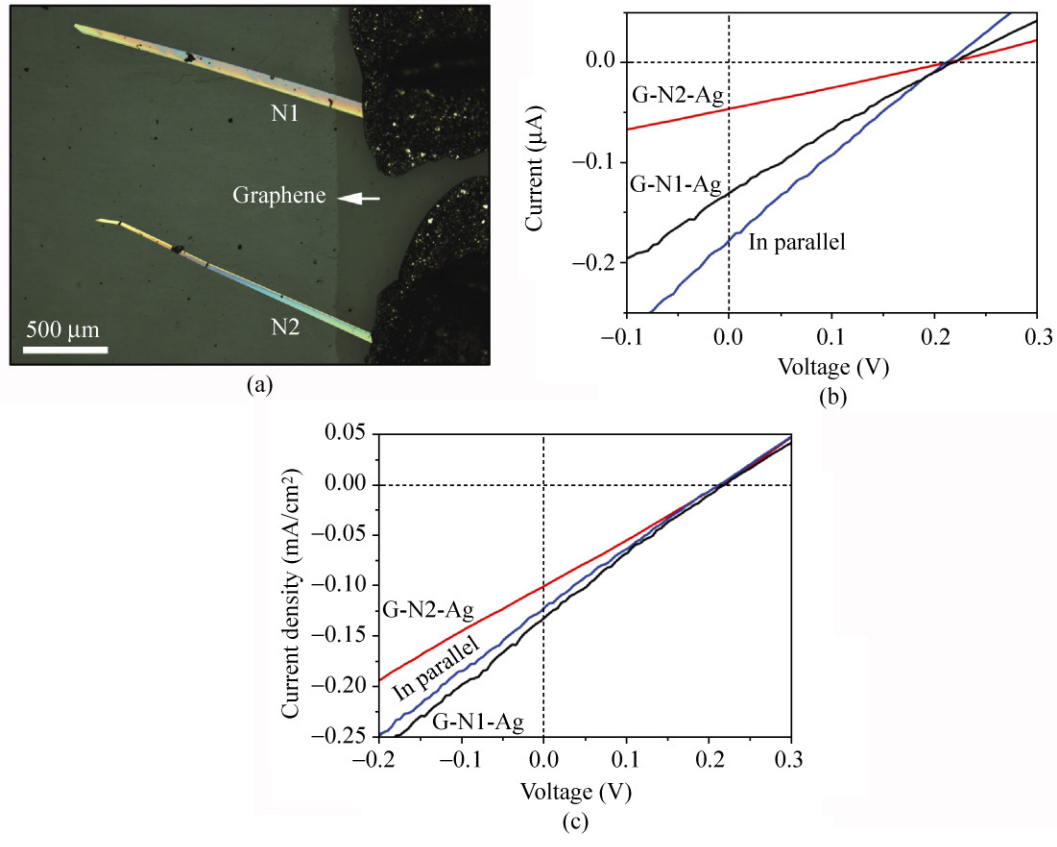

Figure 5 Solar cells based on two parallel CdSe nanobelts. (a) Optical image of the device with two CdSe nanobelt in parallel, both of which are covered by the same graphene film on the left portion and separated Ag paste contacts on their right ends. (b) *I–V* curves of cells based on individual nanobelts (N1, N2), and their parallel connection. (c) *J–V* curves of the above cells calculated based on the junction areas of G–N1 and G–N2, respectively, and the total junction area for parallel connection

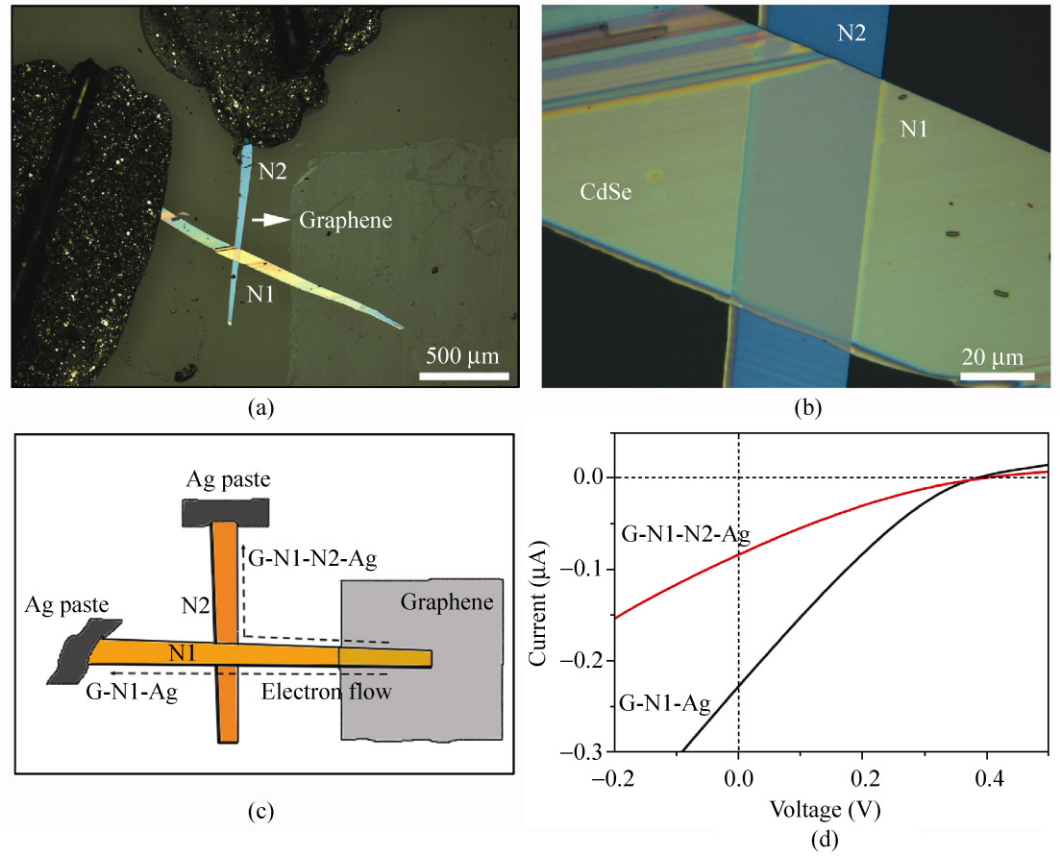

Figure 6 Solar cells based on two CdSe nanobelts arranged in series. (a) Optical image of the device containing two contacted nanobelts (N1, N2), a graphene film covering the right end of N1, and Ag pastes connected to the ends of N1 and N2. (b) Close view of the contact area between N1 and N2, showing smooth overlapping of these two nanobelts. (c) Illustration of the two cell configurations G–N1–Ag and G–N1–N2–Ag, where electrons flow through only N1 to the Ag paste in the former cell, while electrons must flow through N1 and N2 in the latter. (d) *I*–*V* curves of the cells G–N1–Ag and G–N1–N2–Ag

the contact resistance between N1 and N2 could be a bottleneck for efficient charge transport. As expected, the cell G–N1–N2–Ag shows a smaller I_{sc} (0.09 μA) compared with the cell G–N1–Ag (0.23 μA) in which electrons move straightforwardly to the Ag electrode along N1 (Fig. 6(d)). One can imagine further reduced output current if more nanobelts are connected in series, which would limit the applications of large area nanobelt networks in photovoltaics. Despite this, the cell performance based on assembled nanobelt networks might be maintained by reducing the contact resistance and optimizing the device configuration.

4. Conclusions

We have used two-dimensional nanostructures (nanobelts and graphene) to fabricate Schottky junction solar cells with high environmental stability. Various device structures including graphene–CdSe cross junctions, nanobelts contacted by graphene or CNTs at the ends, and nanobelts in parallel or series, have been demonstrated. Our solar cell structures can be extended to include other semiconducting nanobelts or nanowires with high carrier mobility and desired optical bandgaps. Large-scale cell integration might be possible based on a large number of self-assembled nanobelts and patterned graphene or CNT films in a predefined configuration.

Acknowledgements

This work was supported by the National Science Foundation of China (NSFC) under grant number 51072005. H. W. Zhu acknowledges the support by the

National Science Foundation of China (No. 50972067), Tsinghua National Laboratory for Information Science and Technology (TNList) Cross-discipline Foundation and Foundation for the Authors of National Excellent Doctoral Dissertations (No. 201038). We acknowledge Yan Li from College of Chemistry in Peking University for help in Raman measurement.

Electronic Supplementary Material: Supplementary material (detailed synthesis procedures and parameters of CdSe nanobelts, graphene films and carbon nanotubes, fabrication process of graphene–CdSe solar cells with various configurations, TEM image of graphene films, optical images and performances of solar cells in other configurations.) is available in the online version of this article at http://dx.doi.org/10.1007/s12274-011-0145-6

References

[1] Yang, P. D.; Yan, R. X.; Fardy, M. Semiconductor nanowire: What's next? *Nano Lett.* **2010**, *10*, 1529–1536.

[2] Novoselov, K. S.; Geim, A. K.; Morozov, S. V.; Jiang, D.; Zhang, Y.; Dubonos, S. V.; Grigorieva, I. V.; Firsov, A. A. Electric field effect in atomically thin carbon films. *Science* **2004**, *306*, 666–669.

[3] Geim, A. K. Graphene: Status and prospects. *Science* **2009**, *324*, 1530–1534.

[4] Cao, Q.; Rogers, J. A. Ultrathin films of single-walled carbon nanotubes for electronics and sensors: A review of fundamental and applied aspects. *Adv. Mater.* **2009**, *21*, 29–53.

[5] Kempa, T. J.; Tian, B. Z.; Kim, D. R.; Hu, J. S.; Zheng, X. L.; Lieber, C. M. Single and tandem axial p-i-n nanowire photovoltaic devices. *Nano Lett.* **2008**, *8*, 3456–3460.

[6] Chen, Z. H.; Appenzeller, J.; Lin, Y. M.; Sippel-Oakley, J.; Rinzler, A. G.; Tang, J. Y.; Wind, S. J.; Solomon, P. M.; Avouris, P. An integrated logic circuit assembled on a single carbon nanotube. *Science* **2006**, *311*, 1735.

[7] Bai, J. W.; Zhong, X.; Jiang, S.; Huang, Y.; Duan, X. F. Graphene nanomesh. *Nat. Nanotechnol.* **2010**, *5*, 190–194.

[8] Li, X. L.; Wang, X. R.; Zhang, L.; Lee, S. W.; Dai, H. J. Chemically derived, ultrasmooth graphene nanoribbon semiconductors. *Science* **2008**, *319*, 1229–1232.

[9] Zhai, T. Y.; Liu, H. M.; Li, H. Q.; Fang, X. S.; Liao, M. Y.; Li, L.; Zhou, H. S.; Koide, Y.; Bando, Y.; Goberg, D. Centimeter-long V_2O_5 nanowires: From synthesis to field-emission, electrochemical, electrical transport, and photoconductive properties. *Adv. Mater.* **2010**, *22*, 2547–2552.

[10] Wen, Q.; Qian, W. Z.; Nie, J. Q.; Cao, A. Y.; Ning, G. Q.; Wang, Y.; Hu, L.; Zhang, Q.; Huang, J. Q.; Wei, F. 100 mm Long, semiconducting triple-walled carbon nanotubes. *Adv. Mater.* **2010**, *22*, 1867–1871.

[11] Wang, X. S.; Li, Q. Q.; Xie, J.; Jin, Z.; Wang, J. Y.; Li, Y.; Jiang, K. L.; Fan, S. S. Fabrication of ultralong and electrically uniform single-walled carbon nanotubes on clean substrates. *Nano Lett.* **2009**, *9*, 3137–3141.

[12] Bae, S.; Kim, H.; Lee, Y.; Xu, X. F.; Park, J. S.; Zheng, Y.; Balakrishnan, J.; Lei, T.; Kim, H. R.; Song, Y. I.; Kim, Y. J.; Kim, K. S.; Ozyilmaz, B.; Ahn, J. H.; Hong, B. H.; Iijima, S. Roll-to-roll production of 30-inch graphene films for transparent electrodes. *Nat. Nanotechnol.* **2010**, *5*, 574–578.

[13] Li, X. S.; Cai, W. W.; An, J. H.; Kim, S.; Nah, J.; Yang, D. X.; Piner, R.; Velamakanni, A.; Jung, I.; Tutuc, E.; Banerjee, S. K.; Colombo, L.; Ruoff, R. S. Large-area synthesis of high-quality and uniform graphene films on copper foils. *Science* **2009**, *324*, 1312–1314.

[14] De Arco, L. G.; Zhang, Y.; Schlenker, C. W.; Ryu, K.; Thompson, M. E.; Zhou, C. W. Continuous, highly flexible, and transparent graphene films by chemical vapor deposition for organic photovoltaics. *ACS Nano* **2010**, *4*, 2865–2873.

[15] Pattantyus-Abraham, A. G.; Kramer, I. J.; Barkhouse, A. R.; Wang, X. H.; Konstantatos, G.; Debnath, R.; Levina, L.; Raabe, I.; Nazeeruddin, M. K.; Gratzel, M.; Sargent, E. H. Depleted-heterojunction colloidal quantum dot solar cells. *ACS Nano* **2010**, *4*, 3374–3380.

[16] Guo, C. X.; Yang, H. B.; Sheng, Z. M.; Lu, Z. S.; Song, Q. L.; Li, C. M. Layered graphene/quantum dots for photovoltaic devices. *Angew. Chem. Int. Ed.* **2010**, *49*, 3014–3017.

[17] Tian, B. Z.; Zheng, X. L.; Kempa, T. J.; Fang, Y.; Yu, N. F.; Yu, G. H.; Huang, J. L.; Lieber, C. M. Coaxial silicon nanowires as solar cells and nanoelectronic power sources. *Nature* **2007**, *449*, 885–889.

[18] Fan, Z. Y.; Razavi, H.; Do, J. W.; Moriwaki, A.; Ergen, O.; Chueh, Y. L.; Leu, P. W.; Ho, J. C.; Takahashi, T.; Reichertz, L. A.; Neale, S.; Yu, K.; Wu, M.; Ager, J. W.; Javey, A. Three-dimensional nanopillar-array photovoltaics on low-cost and flexible substrates. *Nat. Mater.* **2009**, *8*, 648–653.

[19] Tak, Y.; Hong, S. J.; Lee, J. S.; Yong, K. Fabrication of ZnO/CdS core/shell nanowire arrays for efficient solar energy conversion. *J. Mater. Chem.* **2009**, *19*, 5945–5951.

[20] Li, X. M.; Zhu, H. W.; Wang, K. L.; Cao, A. Y.; Wei, J. Q.; Li, C. Y.; Jia, Y.; Li, Z.; Li, X.; Wu, D. H. Graphene-on-silicon Schottky junction solar cells. *Adv. Mater.* **2010**, *22*, 2743–2748.

[21] Dufaux, T.; Boettcher, J.; Burghard, M.; Kern, K. Photocurrent distribution in graphene–CdS nanowire devices. *Small* **2010**, *6*, 1868–1872.

[22] Ye, Y.; Dai, Y.; Dai, L.; Shi Z. J.; Liu, N.; Wang, F.; Fu, L.; Peng, R. M.; Wen, X. N.; Chen, Z. J.; Liu, Z. F.; Qin, G. G. High-performance single CdS nanowire (nanobelt) Schottky junction solar cells with Au/graphene Schottky electrodes. *ACS Appl. Mater. Interf.* **2010**, *2*, 3406–3410.

[23] Ma, C.; Wang, Z. L. Road map for the controlled synthesis of CdSe nanowires, nanobelts, and nanosaws—A step towards nanomanufacturing. *Adv. Mater.* **2005**, *17*, 2635–2639.

[24] Zhang, L. H.; Jia, Y.; Wang, S. S.; Li, Z.; Ji, C. Y.; Wei, J. Q.; Zhu, H. W.; Wang, K. L.; Wu, D. H.; Shi, E. Z.; Fang, Y.; Cao, A. Y. Carbon nanotube and CdSe nanobelt Schottky junction solar cells. *Nano Lett.* **2010**, *10*, 3583–3589.

[25] Shi, Y. M.; Kim, K. K.; Reina, A.; Hofmann, M.; Li, L. J.; Kong, J. Work function engineering of graphene electrode via chemical doping. *ACS Nano* **2010**, *4*, 2689–2694.

[26] Whang, D.; Jin, S.; Wu, Y.; Lieber, C. M. Large-scale hierarchical organization of nanowire arrays for integrated nanosystems. *Nano Lett.* **2003**, *3*, 1255–1259.

[27] Tao, A.; Kim, F.; Hess, C.; Goldberger, J.; He, R. R.; Sun, Y. G.; Xia, Y. N.; Yang, P. D. Langmuir–Blodgett silver nanowire monolayers for molecular sensing using surface-enhanced Raman spectroscopy. *Nano Lett.* **2003**, *3*, 1229–1233.

[28] Yu, G. H.; Cao, A. Y.; Lieber, C. M., Large-area blown bubble films of aligned nanowires and carbon nanotubes. *Nat. Nanotechnol.* **2007**, *2*, 372–377.